



PZR Coordinates Shp2 Noonan and LEOPARD Syndrome Signaling in Zebrafish and Mice

Citation

Paardekooper Overman, J., J.-S. Yi, M. Bonetti, M. Soulsby, C. Preisinger, M. P. Stokes, L. Hui, et al. 2014. "PZR Coordinates Shp2 Noonan and LEOPARD Syndrome Signaling in Zebrafish and Mice." *Molecular and Cellular Biology* 34 (15) (May 27): 2874–2889.
doi:10.1128/mcb.00135-14.

Published version

<https://doi.org/10.1128/MCB.00135-14>

Link

<http://nrs.harvard.edu/urn-3:HUL.InstRepos:30203530>

Terms of use

This article was downloaded from Harvard University's DASH repository, and is made available under the terms and conditions applicable to Other Posted Material (LAA), as set forth at

<https://harvardwiki.atlassian.net/wiki/external/NGY5NDE4ZjgzNTc5NDQzMGIzZWZhMGFIOWI2M2EwYTg>

Accessibility

<https://accessibility.huit.harvard.edu/digital-accessibility-policy>

Share Your Story

The Harvard community has made this article openly available.
Please share how this access benefits you. [Submit a story](#)

PZR Coordinates Shp2 Noonan and LEOPARD Syndrome Signaling in Zebrafish and Mice

Jeroen Paardekooper Overman,^a Jae-Sung Yi,^b Monica Bonetti,^a Matthew Soulsby,^b Christian Preisinger,^{c*} Matthew P. Stokes,^d Li Hui,^d Jeffrey C. Silva,^d John Overvoorde,^a Piero Giansanti,^c Albert J. R. Heck,^c Maria I. Kontaridis,^e Jeroen den Hertog,^{a,f} Anton M. Bennett^{b,g}

Hubrecht Institute-KNAW and University Medical Center Utrecht, Utrecht, Netherlands^a; Department of Pharmacology, Yale University School of Medicine, New Haven, Connecticut, USA^b; Department of Biomolecular Mass Spectrometry and Proteomics, Utrecht University, Utrecht, Netherlands^c; Cell Signaling Technology, Danvers, Massachusetts, USA^d; Harvard Medical School, Department of Cardiology, Beth Israel Deaconess Medical Center, Boston, Massachusetts, USA^e; Institute Biology Leiden, Leiden, Netherlands^f; Program in Integrative Cell Signaling and Neurobiology of Metabolism, Yale University School of Medicine, New Haven, Connecticut, USA^g

Noonan syndrome (NS) is an autosomal dominant disorder caused by activating mutations in the *PTPN11* gene encoding Shp2, which manifests in congenital heart disease, short stature, and facial dysmorphism. The complexity of Shp2 signaling is exemplified by the observation that LEOPARD syndrome (LS) patients possess inactivating *PTPN11* mutations yet exhibit similar symptoms to NS. Here, we identify “protein zero-related” (PZR), a transmembrane glycoprotein that interfaces with the extracellular matrix to promote cell migration, as a major hyper-tyrosyl-phosphorylated protein in mouse and zebrafish models of NS and LS. PZR hyper-tyrosyl phosphorylation is facilitated in a phosphatase-independent manner by enhanced Src recruitment to NS and LS Shp2. In zebrafish, PZR overexpression recapitulated NS and LS phenotypes. PZR was required for zebrafish gastrulation in a manner dependent upon PZR tyrosyl phosphorylation. Hence, we identify PZR as an NS and LS target. Enhanced PZR-mediated membrane recruitment of Shp2 serves as a common mechanism to direct overlapping pathophysiological characteristics of these *PTPN11* mutations.

The Src homology 2 (SH2) domain-containing protein tyrosine phosphatase 2 (Shp2) is an ubiquitously expressed non-transmembrane protein tyrosine phosphatase (PTP) encoded by the *PTPN11* gene (1). Shp2 comprises two SH2 domains, a PTP domain and a C-terminal tail that contains a proline-rich region flanked by two tyrosine phosphorylation sites. The SH2 domains of Shp2 serve to direct protein-protein interactions with its upstream phosphotyrosyl target in a sequence-specific context, and the SH2 domains participate in maintaining a closed conformation by establishing contacts with the PTP domain (2). The phosphatase domain of Shp2 catalyzes substrate-specific dephosphorylation and is tightly regulated. In the basal state, the catalytic activity of Shp2 is suppressed by Shp2 assuming a “closed” conformation maintained through the NH₂-terminal SH2 (N-SH2) domain forming surface contacts with the PTP domain, which occludes the catalytic site. SH2 domain engagement disrupts this “closed” conformation, leading to allosteric modulation and exposure of the catalytic site in to an “open” state that is now substrate accessible (2). Engagement of the SH2 domains provides an elegant molecular switch mechanism to activate the phosphatase that allows for targeted substrate dephosphorylation within a precise microenvironment. As such, the repertoire of Shp2-binding proteins plays a major role in dictating Shp2 signaling complexity and specificity. Consistent with this, interference with Shp2’s SH2 domains abrogates both physiological and pathophysiological signaling (3). Thus, the integrity of the SH2 domains of Shp2 plays a critical role in its ability to signal.

A wealth of biochemical, cellular, and genetic evidence in mice, *Drosophila melanogaster*, and zebrafish has established that Shp2 plays a positive signaling role downstream of numerous receptor tyrosine kinases, cytokine receptors, G protein-coupled receptors, and integrins (1). The repertoire of Shp2-interacting proteins in combination with a wide variety of substrates (4) endows this

phosphatase with the capability of engaging a complex array of signaling molecules and pathways, such as the Ras/mitogen-activated protein kinase (MAPK), phosphoinositol 3-kinase (PI3K)/Akt, JAK/STAT, RhoA/Rac, and Src family kinases (SFKs). Shp2 has been shown to promote a number of cellular functions, including cell growth, cell survival, and differentiation, hence affecting organismal functions, such as development in mice (5, 6), *Drosophila* (7), and zebrafish (8). The highly conserved nature of Shp2 signaling in lower organisms has provided powerful model systems for the genetic dissection of Shp2’s function in development. The realization that Shp2 plays an important role in human development arose through the discovery that germ line mutations in the *PTPN11* gene coding for Shp2 cause two similar types of autosomal dominant disorders (9, 10). More than 50% of Noonan syndrome (NS) (NIM163950) cases are caused by mutations in *PTPN11* that result in increased Shp2 catalysis. In contrast, as much as 90% of LEOPARD syndrome (LS) (NIM151100) mutations are caused by inactivating *PTPN11* mutations that give rise to impaired Shp2 activity.

NS and LS are autosomal dominant disorders that manifest in

Received 26 January 2014 Returned for modification 6 February 2014

Accepted 15 May 2014

Published ahead of print 27 May 2014

Address correspondence to Anton M. Bennett, anton.bennett@yale.edu.

* Present address: Christian Preisinger, Proteomics Facility, Interdisciplinary Centre for Clinical Research (IZKF) Aachen, Aachen, Germany.

J.P.O. and J.-S.Y. contributed equally to this article.

J.D.H. and A.M.B. jointly directed the work.

Copyright © 2014, American Society for Microbiology. All Rights Reserved.

doi:10.1128/MCB.00135-14

short stature, ocular hypertelorism, cardiac defects, webbed neck, and increased incidence of mental retardation (11–13). NS and LS comprise part of a larger series of disorders that have thus far been characterized by mutations in components of the Ras/MAPK pathway and are collectively referred to as “RASopathies” (14). As such, NS and LS exhibit overlapping clinical presentations, such as proportionate short stature, facial dysmorphism, musculoskeletal anomalies, and, to a lesser extent, congenital heart disease. Despite the similarities between NS and LS, these “RASopathies” are caused by opposite effects on Shp2 activity (9, 15–18). These observations suggest that NS and LS may utilize common signaling components in the pathogenesis of these developmental disorders. Interestingly, one common feature of both NS and LS mutants is that both forms of Shp2 exhibit an increased propensity to adopt an “open” conformation, leading to increased affinity to upstream target binding through the SH2 domains and target substrates (2, 8, 19, 20). Hence, the “open” conformation of NS and LS disease mutants may underlie the molecular pathogenesis of these syndromes rather than altered substrate dephosphorylation by the PTP domain. Despite these highly plausible explanations, it remains unclear how activating and inactivating mutants of Shp2 liberate overlapping disease outcomes. Moreover, the target or targets for both NS and LS that must presumably be shared in order for them to elicit overlapping clinical outcomes are unknown.

PZR (“protein zero related”) is a transmembrane glycoprotein with an extracellular immunoglobulin (Ig) domain and an intracellular domain containing two immunoreceptor tyrosine-based inhibitory motifs (ITIMs) (21–23). The ITIMs, when tyrosyl phosphorylated, serve as Shp2 binding sites (21). We had identified previously that NS-associated Shp2 mutants induce PZR hyper-tyrosyl phosphorylation and recruit increased Shp2 (25). Moreover, in *Ptpn11*^{D61G/+} mouse embryos, PZR is hyper-tyrosyl phosphorylated, demonstrating that it is aberrantly regulated in NS mice during development. Interestingly, PZR is upregulated during blastocyst formation (24). Moreover, in mouse embryo fibroblasts derived from NS mice, adhesion-dependent extracellular signal-regulated kinase 1/2 (ERK1/2) activation is abrogated upon loss of PZR expression (25).

To gain further insight into how NS and LS might liberate similar phenotypes, we performed an unbiased phosphotyrosine proteomics screen in a mouse model of NS and a zebrafish model of NS and LS. We identified PZR as a major hyper-tyrosyl-phosphorylated protein in both NS and LS in mice and zebrafish. The role of PZR in development remains unclear, and the pathophysiological significance of PZR-Shp2 interactions in NS and LS is also unknown. NS and LS are linked to defects in gastrulation cell movements, and Shp2 is essential for gastrulation movements in mice and zebrafish (11, 26). We show that PZR-Shp2 interactions are required for gastrulation in zebrafish. These results define a functional role for PZR in an intact organism. Moreover, they suggest that PZR is a common target that contributes to altered development in cases of both NS and LS.

MATERIALS AND METHODS

DNA constructs and cloning. *Ptpn11* was cloned previously (11). *Mpz11* was cloned by nested PCR from zebrafish embryo cDNA (from bud stage to 48 h postfertilization [hpf]) with Phusion DNA polymerase (Finnzymes, Vantaa, Finland) using fwPZRout (5′-GGGCGTTATTCATGAAATCTAAA-3′), rvPZRout (5′-CTCAGGTTGGCAGAGATGT-3′),

fwPZRstart (5′-GCGGATCCATGGAATAAGGCTT-3′), and rvPZRstop (5′-GCCGAATTCTCAGTTCTTGC GGATG-3′). The PCR product was cloned into pCS2+ using BamHI and EcoRI. PZR ITIM Y236F, Y258F, and Y236F Y258F mutants were made using site-directed mutagenesis with the following primers (boldfacing indicates introduced mutations in the primer sequence): Fw_Y>F236_PZR (5′-GGACCGGTGATTTTCGCTCAGCTCGAT-3′), Rv_Y>F236_PZR (5′-ATCGAGCTGAGCGAAAATCACCGGTCC-3′), and RvstopY258F (5′-CCGAATTCTCAGTTCTTGC GGATGCTGCGAACACACCGGCTC-3′). PZR was then subcloned using BamHI and XhoI restriction enzymes into pSG5 vector encoding an RPTPa signal sequence and hemagglutinin (HA) tag (27) using the following primers: FwBamHI AGVSDPZR (5′-GCCGGATCCGCCGGGGTCTCAGAT-3′) and RvXhoI stopPZR (5′-GCCCTCGAGTCTTTCGCGGAT-3′).

Antibodies, chemicals, cell lines, and expression reagents. Rabbit monoclonal phospho-PZR(Y241) and rabbit monoclonal phospho-PZR(Y263) antibodies were generated in collaboration with Cell Signaling. Mouse monoclonal Src antibody, rabbit polyclonal Src antibody, rabbit polyclonal phospho-ERK1/2(T202 Y204), mouse monoclonal ERK1/2 antibody, rabbit polyclonal phospho-Akt(S473) antibodies and mouse monoclonal Akt antibodies were purchased from Cell Signaling. Rabbit polyclonal Shp2 antibodies and rabbit polyclonal ERK1/2 antibody were purchased from Santa Cruz Biotechnology. Mouse monoclonal Shp2 antibody was purchased from BD Bioscience. Rabbit polyclonal PZR (105-6) was generously provided by Z. J. Zhao. Src family kinase inhibitors PP2 and SU6656 were purchased from Calbiochem. HEK-293, NIH 3T3, SYF (*Src*^{-/-} *Yes*^{-/-} *Fyn*^{-/-} mouse embryonic fibroblasts [MEFs]), and *Src*^{+/+} (*Src*-overexpressing SYF) cells were purchased from ATCC and grown in growth medium (Dulbecco’s modified Eagle’s medium [DMEM] supplemented with 1% penicillin–streptomycin and 10% fetal bovine serum) in a 5% CO₂ incubator at 37°C. Replication-deficient adenoviral (Ad) constructs harboring wild-type Shp2 (Ad-Shp2 WT), the E76A gain-of-function Shp2 mutant (Ad-Shp2^{E76A}), and green fluorescent protein (GFP) (Ad-GFP) were prepared as previously described (25, 28). NIH 3T3 and SYF cells were infected with by adenovirus at a dosage of 50 multiplicities of infection (MOI). The pJ3Ω vectors containing *Src* WT and the K295R/Y527F dominant-negative *Src* mutant (*Src*^{K295R/Y527F}) have been described in previously (29). The pIRES-GFP plasmids encoding the Shp2 WT, gain-of-function/Noonan syndrome mutants of Shp2 (Shp2^{E76A} and Shp2^{N308D}), and LEOPARD syndrome mutants of Shp2 (Shp2^{Y279C} and Shp2^{T468M}) have been described previously (15, 25). DNA transfection into HEK-293 and SYF cells was performed using Lipofectamine 2000 according to the manufacturer’s protocol. Mouse anti-phosphotyrosine antibody 4G10 (05-321) was from Merck Millipore, rabbit anti-GFP (TP401) was from Acris, and mouse anti-HA.11 clone 16B12 was from Covance.

Animal handling. *Ptpn11*^{D61G/+} mice were provided by Benjamin Neel (University of Toronto, Toronto, Ontario, Canada) and were genotyped as described previously (30). Briefly, *Ptpn11*^{D61G/+} male mice were crossed with WT C75BL/6 × SV129 female mice, and their offspring were genotyped by PCR and digestion with AgeI for the D61G allele. Animal handling was approved by the Yale University Institutional Animal Care and Use Committee. Tissues from *Ptpn11*^{Y279C/+} mice were provided by Maria Kontaridis (Harvard University, Boston, MA).

In situ hybridization. Zebrafish were kept and embryos were staged as described by Westerfield (31). *In situ* hybridizations were performed as described by Thisse et al. (32). The *bmp2b*, *chd*, *gsc*, *ntla*, *dlx3*, *hgg*, *krox20*, and *myod* probes were described previously (11, 33). Antisense and sense *Mpz11* probes, respectively, were synthesized by T7 and SP6 mRNA polymerase (Promega) from pCS2+PZR.

MO RNA and injections. Zebrafish were kept and embryos were injected at the 1-cell stage. PZR morpholino oligonucleotide (MO) 5′-CAGAGACCCTTACTGTGGTGGGACGC-3′, Shp2 MO 5′-GGTGGAACCA CCTTCGGGATGTCAT-3′, *nacre* MO 5′-CATGTTCAACTATGTGTTA GCTTCA-3′, and standard p53 MO were from Genetools (Philomath,

OR). 5'-capped sense synthetic mRNA was synthesized with SP6 or T7 mRNA polymerase using the mMessage mMachine kit from Ambion. The amount of RNA that was injected at the 1-cell stage was optimized for each synthetic RNA. MOs were titrated down to give a specific phenotype without inducing increased apoptosis as coinjection of 1 nmol p53 MO did not attenuate the phenotype. Likewise, mRNA was titrated down to either induce a phenotype or rescue an MO-induced phenotype.

Immunoprecipitation and immunoblotting. Cells were lysed on ice in lysis buffer (20 mM Tris-HCl, 150 mM NaCl, 1 mM CaCl₂, 1 mM MgCl₂, 1% Nonidet P-40, 1 mM Na₃VO₄, 10 mM NaF, 1 mM benzamidine, 1 mM phenylmethylsulfonyl fluoride [PMSF], 1 μg/ml pepstatin A, 5 μg/ml aprotinin, 5 μg/ml leupeptin). Tissues from Noonan syndrome (NS) and LEOPARD syndrome (LS) mice were lysed by homogenization with lysis buffer. Cell or tissue lysates were incubated at 4°C for 30 min and clarified by centrifugation at 14,000 rpm at 4°C for 10 min. The protein concentration was determined using the bicinchoninic acid (BCA) reagent according to the manufacturer's instructions (Pierce). For immunoprecipitations, 500 μg of lysate was incubated with 1 μg of the indicated antibodies at 4°C overnight. Immune complexes were collected on either protein A- or protein G-Sepharose beads for 4 h at 4°C, washed three times with the same lysis buffer, and then heated to 95°C in sample buffer for 5 min. Total cell or tissue lysates and immune complexes were subjected to SDS-PAGE and immunoblotting. The sites of antibody binding were visualized using enhanced chemiluminescence detection or the Odyssey imaging system.

Transfected cells were lysed in radioimmunoprecipitation assay (RIPA) buffer (150 mM NaCl, 20 mM Tris [pH 8.0], 10 mM Na₂HPO₄, 5 mM EDTA, 1 mM Na-orthovanadate, 10% glycerol, 1% Nonidet P-40, 1% sodium deoxycholate, 0.1% SDS, 2.5 mM sodium fluoride, 5 μM β-glycerophosphate, 1 μg/ml aprotinin, 1 μg/ml leupeptin) for 15 min on ice at 1 ml per 10-cm-diameter dish. Samples were centrifuged for 30 min at 14,000 rpm at 4°C. The samples were precleared using protein A-agarose beads for 1 h, and an aliquot of whole-cell lysate was immunoprecipitated with 1 μg antibody against HA for approximately 1 h on ice. Samples were precipitated using 25 μl protein A-agarose slurry for approximately 1 h at 4°C. Samples were boiled in 2× Laemmli buffer, and SDS-PAGE was performed.

For zebrafish, bud-stage embryos were snap-frozen in liquid nitrogen and stored at -80°C. Subsequently embryos were ground in cell lysis buffer containing 50 mM Tris (pH 7.5), 150 mM NaCl, 1 mM EDTA, 1 mM sodium orthovanadate, 1% Nonidet P-40, 0.1% sodium deoxycholate, 2.5 mM sodium fluoride, 5 mM β-glycerophosphate, 1 μg/ml aprotinin, and 1 μg/ml leupeptin. Samples were then boiled in Laemmli sample buffer containing 4% SDS and β-mercaptoethanol. Proteins equivalent to 4 embryos per lane were subjected to SDS-PAGE and blotted onto a polyvinylidene difluoride (PVDF) membrane. After blotting, membranes were stained using Coomassie blue to verify equal loading. 293T cells were maintained in Dulbecco's modified Eagle's medium (DMEM) or Ham's F-12 medium containing 10% penicillin-streptomycin and 7.5% fetal calf serum (FCS), respectively. For serum starvation experiments, nonessential amino acids were added. 293T and COS7 cells were passed twice a week at 1:20 and 1:7 before transfection. Transfection of zebrafish PZR was performed using polyethylenimine (PEI) from Sigma with 20 μg DNA. After transfection overnight, medium was replaced with serum and harvested 40 h after transfection.

MS analysis. The PhosphoScan method was performed as previously described (34–37). Wild-type and Shp2 mutant (Noonan syndrome) mouse hearts were homogenized, sonicated, and centrifuged to remove cellular debris. Total protein for each tissue was normalized using the ProteinPlus Coomassie reagent (Pierce), and proteins were reduced, alkylated, and digested overnight using trypsin (Worthington). The resulting peptides were separated from nonpeptide material by solid-phase extraction with Sep-Pak classic C₁₈ cartridges (Waters). Lyophilized peptides were redissolved, and phosphopeptides were enriched by immunoaffinity purification using pY-100 phosphotyrosine antibody (9411; Cell Signal-

ing Technology). Peptides were eluted with 0.15% trifluoroacetic acid (TFA) and concentrated with C₁₈ spin tips immediately prior to liquid chromatography-mass spectrometry (LC-MS) analysis.

Duplicate injections of each sample were run to generate analytical replicates and increase the number of tandem MS (MS/MS) identifications from each sample. Peptides were loaded directly onto a 10-cm by 75-μm PicoFrit capillary column packed with Magic C₁₈ AQ reversed-phase resin. The column was developed with a 45-min linear gradient of acetonitrile in 0.125% formic acid delivered at 280 nl/min. Tandem mass spectra were collected with an LTQ-Orbitrap XL mass spectrometer running XCalibur using a Top 10 method, a dynamic exclusion repeat count of 1, and a repeat duration of 30 s. MS spectra were collected in the Orbitrap component of the mass spectrometer, and MS/MS spectra were collected in the LTQ portion.

MS/MS spectra were processed using SEQUEST and the Core platform (Gygi Lab, Harvard University) (38–41). Searches were performed against the mouse NCBI database, with reverse decoy databases included for all searches to estimate false-positive rates. Peptide assignments were obtained using a 0.98-precision cutoff in the linear discriminant analysis module of Core. Cysteine carboxamidomethylation was specified as a static modification, and methionine oxidation and serine, threonine, and tyrosine phosphorylation were allowed. Results were further narrowed using mass accuracy (±5-ppm) filters and the presence of a phosphotyrosine in the peptide. Label-free quantitation was performed using Progenesis v4.1 (Nonlinear Dynamics). Peptide abundance data were manually reviewed in Progenesis for all peptides with at least a 2.0-fold change to ensure accuracy of results.

Global phosphotyrosine differential proteomic analysis in the zebrafish heart. Heart tissue was lysed in urea buffer (20 mM HEPES [pH 8.0], 9 M urea, 1 mM sodium vanadate, 2.5 mM sodium pyrophosphate, 1 mM β-glycerophosphate). The lysate was sonicated and clarified by centrifugation. Tissue lysate was reduced by dithiothreitol (DTT) and alkylated with iodoacetamide. Samples were then diluted 4 times with 20 mM HEPES to reduce the urea concentration to 2 M and digested by trypsin overnight at room temperature with gentle shaking. Phosphotyrosine-containing peptides were isolated using immobilized phosphotyrosine-specific antibody PY100 (PhosphoScan kit; Cell Signaling Technology). Following immunopurification, phosphotyrosine-containing peptides were analyzed by LC-MS/MS as described previously (37).

RESULTS

PZR is a major hyper-tyrosyl-phosphorylated protein in NS.

Since NS and LS exhibit overlapping clinical outcomes, we set out to identify target proteins that are affected by both syndromes. We hypothesized that targets similarly altered in their levels of tyrosyl phosphorylation in both NS and LS likely represent molecules of convergence in these diseases. Given that NS and LS mutants exhibit opposite catalytic activities, we reasoned that a phosphatase-independent mechanism likely represents a common pathway for these two syndromes. Therefore, we focused on the identification of hyper-tyrosyl-phosphorylated proteins in a mouse model of NS rather than hypo-tyrosyl-phosphorylated ones, since the latter likely represents phosphatase-dependent Shp2 substrates.

We performed a phosphotyrosyl proteomics screen in mice harboring a knock-in of an NS-associated Shp2 mutant (30). Mice containing an Asp61 to Gly61 (D61G) mutation within the NH₂-terminal SH2 domain of Shp2 (Shp2^{D61G}) generate an NS mutation found in humans (9). Heterozygous progeny of these mice (*Ptpn11*^{D61G/+}) recapitulate several NS features observed in humans, such as cardiovascular and skeletal abnormalities (30). Since both NS and LS patients exhibit significant clinical defects in the heart we focused on this tissue. We performed a global survey of the levels of tyrosyl-phosphorylated proteins in the hearts of

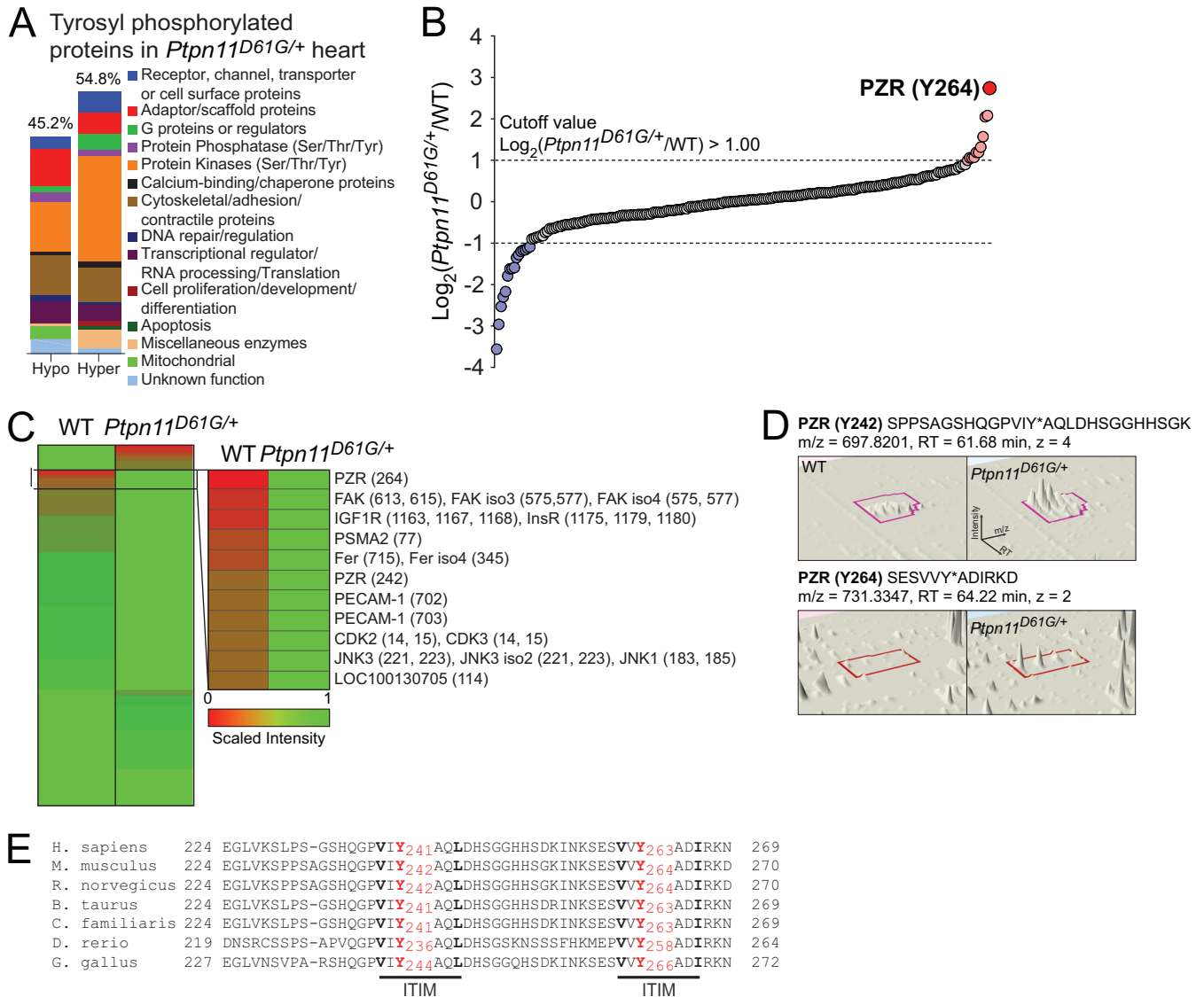


FIG 1 Proteomic analysis of differentially tyrosyl-phosphorylated proteins in hearts of *Ptpn11*^{D61G/+} mice. (A) Classification of hypo- and hyper-tyrosyl-phosphorylated proteins in the hearts of *Ptpn11*^{D61G/+} mice. (B) Log₂-transformed values for the ratio of each phosphotyrosine-containing peptide in wild-type and *Ptpn11*^{D61G/+} mouse hearts. (C) Heat map of differentially tyrosyl-phosphorylated peptides (the site of phosphorylation is identified by MS in parentheses). (D) Extracted ion chromatogram and peptide sequence of PZR-containing tyrosine 242 (upper panels) and tyrosine 264 (lower panels) by differential proteomics. (E) Amino acid sequences of the PZR C terminus in different vertebrates. Consensus sequences for ITIM (S/I/V/L/YXXXI/V/L) are indicated in boldface, and tyrosine residues are marked red with the appropriate amino acid numbering. Sequences are shown for the PZR C terminus from *Homo sapiens*, *Mus musculus*, *Rattus norvegicus*, *Bos taurus*, *Canis lupus familiaris*, *Danio rerio*, *Gallus gallus*.

5-day-old wild-type and *Ptpn11*^{D61G/+} mice using an immunofluorescence phosphoproteomics approach (34). The relative abundance of tyrosyl-phosphorylated proteins was assessed by quantitating the frequency of phosphopeptides derived from wild-type and *Ptpn11*^{D61G/+} mice (34). We identified an approximately equal repertoire of differentially hypo- and hyper-tyrosyl-phosphorylated peptides in the hearts of *Ptpn11*^{D61G/+} mice (Fig. 1A and B). The limited number of differentially tyrosyl-phosphorylated peptides suggests that the NS mutant induces a discrete influence on global tyrosyl phosphorylation levels in the heart (Fig. 1B). The highest induced hyper-tyrosyl-phosphorylated peptide represented Y264, which is present in the transmembrane glycoprotein “protein zero-related” (PZR) and was induced by 6.7-fold com-

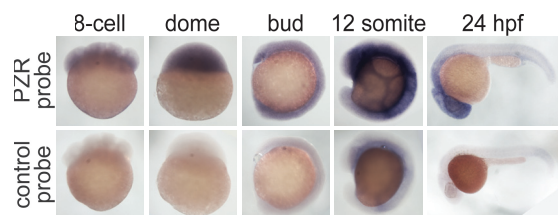


FIG 2 Expression pattern of PZR in developing zebrafish. *In situ* hybridization for PZR was performed on developing zebrafish embryos at the 8-cell, dome, bud, and 12-somite stages and at 24 hpf. The PZR sense probe was used as a control.

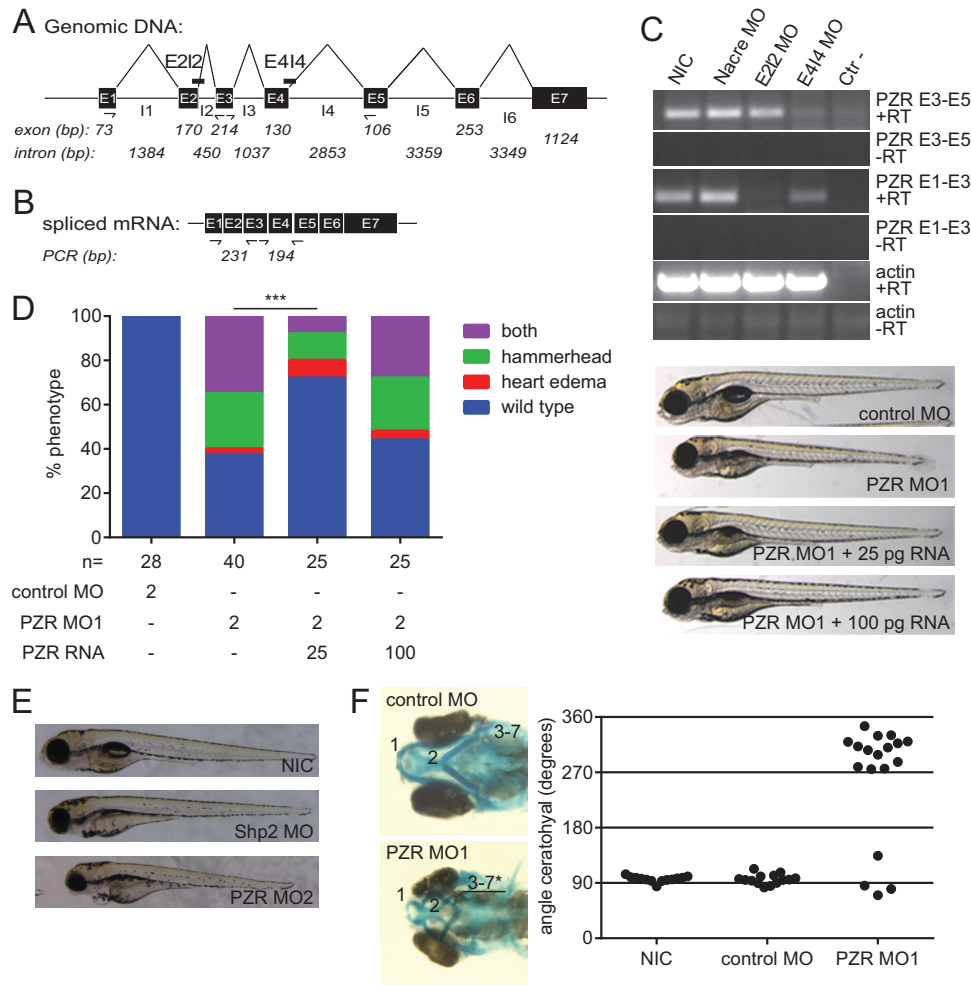


FIG 3 PZR is required for zebrafish development. (A) Genomic organization of the zebrafish *mpz1* gene encoding PZR. The target sites of E414 MO (PZR MO1) and E212 MO (PZR MO2) are indicated as well as the positions of the oligonucleotides used for amplification of E3/E5 and E1/E3. (B) PZR mRNA and the positions of the oligonucleotides used for reverse transcription-PCR (RT-PCR) are depicted; the sizes (bp) of the PCR products are shown. (C) Embryos were untreated (noninjected control [NIC]) or injected at the 1-cell stage with the control MO (nacre MO), PZR E212MO (PZR MO2), or E414 MO (PZR MO1). PCR was performed for E3/E5, or E1/E3. Ctr-, water control. (D) Embryos were injected (1-cell stage) with 2 pg control MO or PZR MO or were coinjected with 25 or 100 pg PZR mRNA. Embryos were scored at 4 dpf. (E) Zebrafish embryos were injected at the 1-cell stage with 2 ng Shp2 MO, PZR MO2, or the control MO and photographed at 3 dpf. (F) Embryos were injected at the 1-cell stage with 2 pg PZR MO or the control MO or noninjected as a control, fixed at 4 dpf, and stained with alcian blue. Meckel's cartilage (no. 1), the ceratohyal (no. 2), and the branchial arches (no. 3 to 7) are indicated. The angle of the ceratohyal was measured.

pared to that in the wild-type controls (Fig. 1C and D). The sequence surrounding Y264 was identified to be part of the immunoreceptor tyrosine inhibitory motif (ITIM) of PZR (23). PZR contains two ITIMs, both of which are highly conserved among vertebrates and when phosphorylated bind directly to the SH2 domains of Shp2 (23). Notably, the other tyrosine-containing ITIM on PZR represented by Y242 was also detected to be hyper-tyrosyl phosphorylated by 2.2-fold (Fig. 1C and D). For clarity, we will use the human amino acid numbering of PZR (Fig. 1E). (Mouse Y242 and Y264 correspond to human Y241 and Y263, respectively.) Previously, we found that PZR was hyper-tyrosyl phosphorylated during embryogenesis in *Ptpn11*^{D61G/+} mice (25). These results identify Y242 and Y264 as sites of PZR hyper-tyrosyl phosphorylation in this mouse model of NS.

Zebrafish have been shown to recapitulate both NS and LS phenotypes (11). Therefore, phosphotyrosyl proteomics screens

were performed in developing (26 days postfertilization) embryos to identify differentially tyrosyl-phosphorylated peptides between zebrafish embryos expressing either NS or LS mutants compared with controls. When injected with the Shp2^{D61G} NS mutant, peptides representing the ITIMs of zebrafish PZR containing Y241 and Y263 were identified to be among the highest-induced phosphotyrosyl-containing peptides (7.7- and 4.7-fold increases for Y241 and Y263, respectively, compared with controls). In addition, LS-injected embryos also were found to contain PZR hyper-tyrosyl-phosphorylated peptides at both Y241 and Y263, representing increases of 3.4- and 3.1-fold relative to wild-type controls. These results identify PZR as a major hyper-tyrosyl-phosphorylated target in zebrafish embryos expressing either NS or LS mutations.

PZR is expressed ubiquitously and functions in the Shp2 pathway in zebrafish. Our data demonstrate that PZR tyrosyl

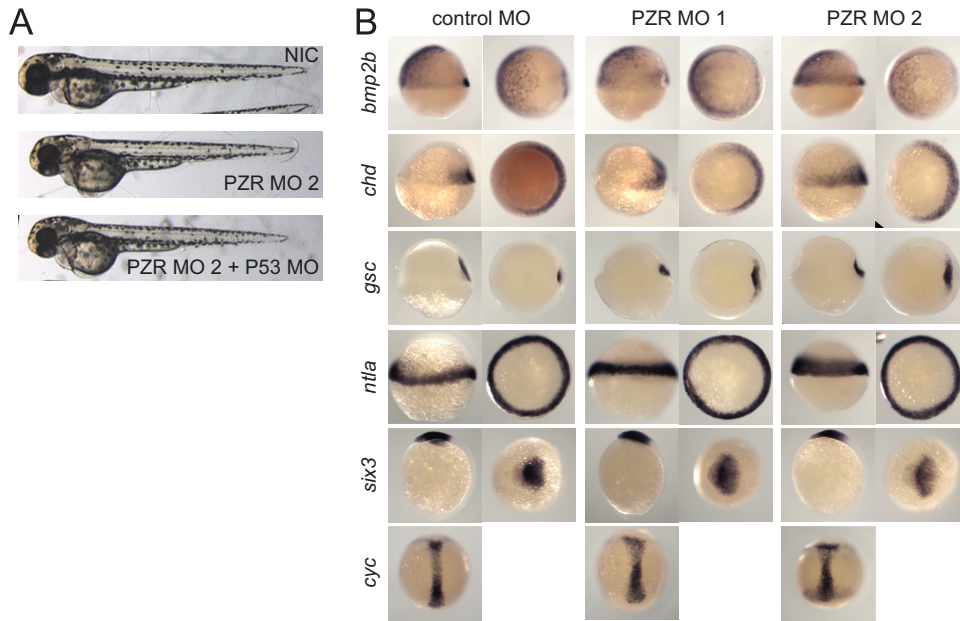


FIG 4 PZR knockdown is specific and does not affect cell specification (A) Zebrafish embryos were injected at the 1-cell stage with 2 ng PZR MO alone or coinjected with p53 morpholino oligonucleotide (MO) and photographed at 2 dpf. (B) Zebrafish embryos were injected at the 1-cell stage with 2 ng PZR MO1, PZR MO2, or control MO and fixed at the shield stage (*bmp2b*, *chd*, *gsc*, and *ntl*), 70% epiboly (*cyc*), and bud stage (*six3*) and probed for cell fate markers by *in situ* hybridization.

phosphorylation is aberrantly regulated in NS mouse embryos and postdevelopmentally in NS hearts (25) (Fig. 1) and during development of NS/LS-expressing zebrafish embryos. These results suggest that altered PZR tyrosyl phosphorylation may play a role in NS and LS pathogenesis. To further examine the role of PZR during zebrafish development, we determined the expression of *mpz11*, the gene encoding zebrafish PZR. Zebrafish PZR was cloned and was used to generate an *mpz11*-specific probe. *In situ* hybridization of *mpz11* expression was apparent from the 8-cell stage onwards, indicating maternal expression. *mpz11* expression was ubiquitous until the bud stage, and at later stages, *mpz11* expression appeared to be enhanced anteriorly (Fig. 2). The specificity of the antisense *mpz11* probe was confirmed by the lack of signal of the sense control probe (Fig. 2). Thus, PZR is maternally

contributed and expressed at embryonic stages during and after zebrafish gastrulation.

PZR knockdown phenocopies NS and LS expression in zebrafish embryos. Next, PZR was knocked down in order to investigate the role of PZR in zebrafish signaling. The specificity of the PZR MO to block PZR splicing was confirmed (Fig. 3A to C). Knockdown of PZR but not a control MO induced a phenotype characterized by a reduced body axis length ($4.9\% \pm 1.1\%$ reduction compared with the control) and heart edema, and this phenotype was confirmed using a second nonoverlapping MO (Fig. 3D and E). Interestingly, similar phenotypes are observed upon Shp2 knockdown in zebrafish (42). Coinjection of a moderate dose of PZR mRNA (25 pg) rescued the PZR MO-induced defects, whereas a higher dose of PZR mRNA (100 pg)

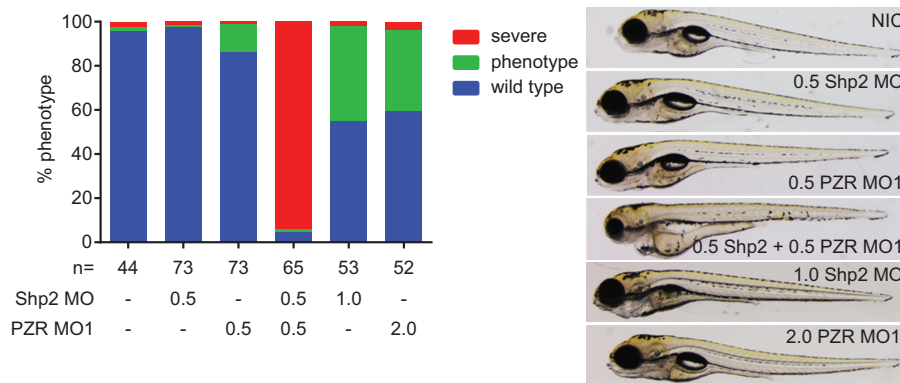


FIG 5 Genetic interaction between Shp2 and PZR. Embryos were injected at the 1-cell stage with Shp2 MO (0.5 pg) or PZR MO (0.5 pg), a combination thereof, or Shp2 MO (1.0 pg) and PZR MO (2.0 pg). Embryos were imaged at 4 dpf. The stacked histogram in the left panel indicates quantitation of the phenotypes shown in representative photographs in the right panel.

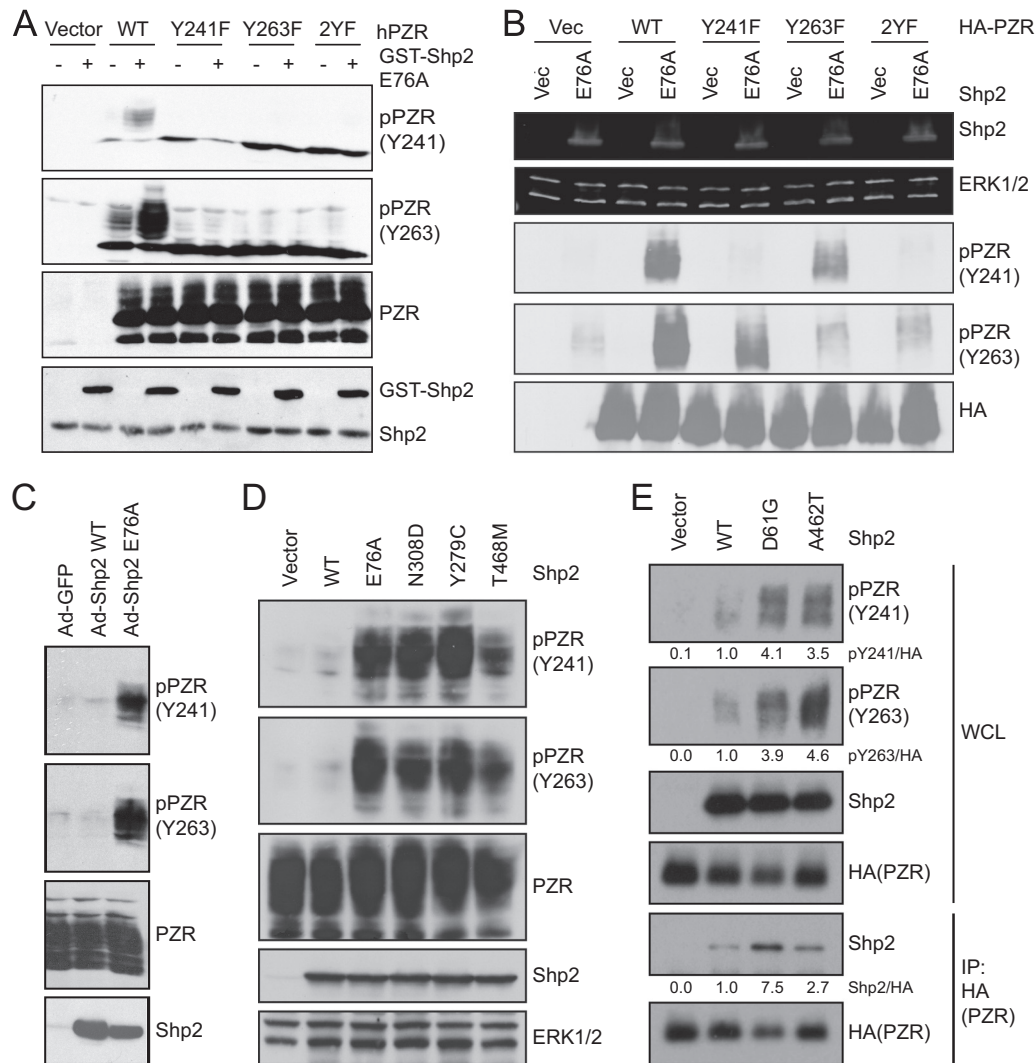


FIG 6 Characterization of PZR tyrosyl phosphorylation. (A) C2C12 cells were cotransfected with empty vector or activated glutathione *S*-transferase (GST)–Shp2^{E76A} and either empty vector (vector), wild-type human PZR (WT), or PZR mutated at tyrosine 242 (Y241F), tyrosine 264 (Y263F), or both (2YF). Cell lysates were immunoblotted with anti-pPZR (Y241 or Y263), -PZR, or -Shp2 antibodies. (B) HEK-293 cells were cotransfected with empty vector (Vec) or activated Shp2^{E76A} and either empty vector (vector), wild-type zebrafish PZR (WT), or PZR mutated at tyrosine 236 (Y241F), tyrosine 258 (Y263F), or both (2YF). Cell lysates were immunoblotted with anti-pPZR (Y241 or Y263), -PZR, or -Shp2 antibodies. ERK1/2 was used as a loading control. (C) HUVECs were infected with adenoviruses expressing either GFP as a control, wild-type Shp2, or Shp2^{E76A}. Cell lysates were immunoblotted with anti-pPZR (Y241 or Y263), anti-total PZR, and anti-Shp2 antibodies. (D) HEK-293 cells were transiently transfected with empty vector, wild-type Shp2 (WT), or the indicated Shp2 mutants (activated Shp2, E76A; NS mutant, N308D; or LS mutants, Y279C and T468M). Cell lysates were immunoblotted with anti-pPZR (Y241 or Y263), -PZR, and -Shp2 antibodies. ERK1/2 was used as a loading control. (E) HEK-293T cells were transfected with HA-tagged zebrafish PZR with empty vector, wild-type Shp2, Shp2^{D61G}, or Shp2^{A462T}. Cell lysates were immunoprecipitated with anti-HA antibodies, and immune complexes were immunoblotted with anti-Shp2 and anti-HA antibodies. Whole-cell lysates (WCL) were blotted with anti-pPZR (Y241 and Y263), -Shp2, and -HA antibodies.

failed to rescue (Fig. 3D). To quantify the craniofacial defects in PZR knockdowns, embryos were fixed at 4 days postfertilization (dpf), and the cartilage was stained with alcian blue. The cartilage was greatly malformed, and the angle of the ceratohyal displayed a significant increase, supporting the notion that PZR knockdown induced craniofacial defects, reminiscent of Shp2 knockdown (11) (Fig. 3F).

The use of knockdown approaches by itself may lead to non-specific activation of p53 and subsequent apoptosis, thereby giving rise to developmental defects (43). To rule out this possibility, we performed a cknockdown of p53 and PZR, which did not attenuate the phenotype (Fig. 4A). We subjected PZR knockdown

embryos to *in situ* hybridization using a panel of cell fate markers at the shield stage (*gsc*, *bmp2b*, *chd*, and *ntl*), 70% epiboly (*cyc*), and bud stage (*six3*). All markers were expressed, indicating that cell specification was not affected (Fig. 4B). Hence, PZR knockdown induced defects similar to those observed in both NS and LS Shp2-expressing embryos.

To investigate the genetic interaction between Shp2 and PZR, we partially knocked down Shp2 and PZR separately and together. If PZR is essential for Shp2 signaling, partial loss of both Shp2 and PZR should induce developmental defects that are more severe than those induced by loss of each alone (42). Knocking down Shp2 and PZR at suboptimal levels did not induce developmental

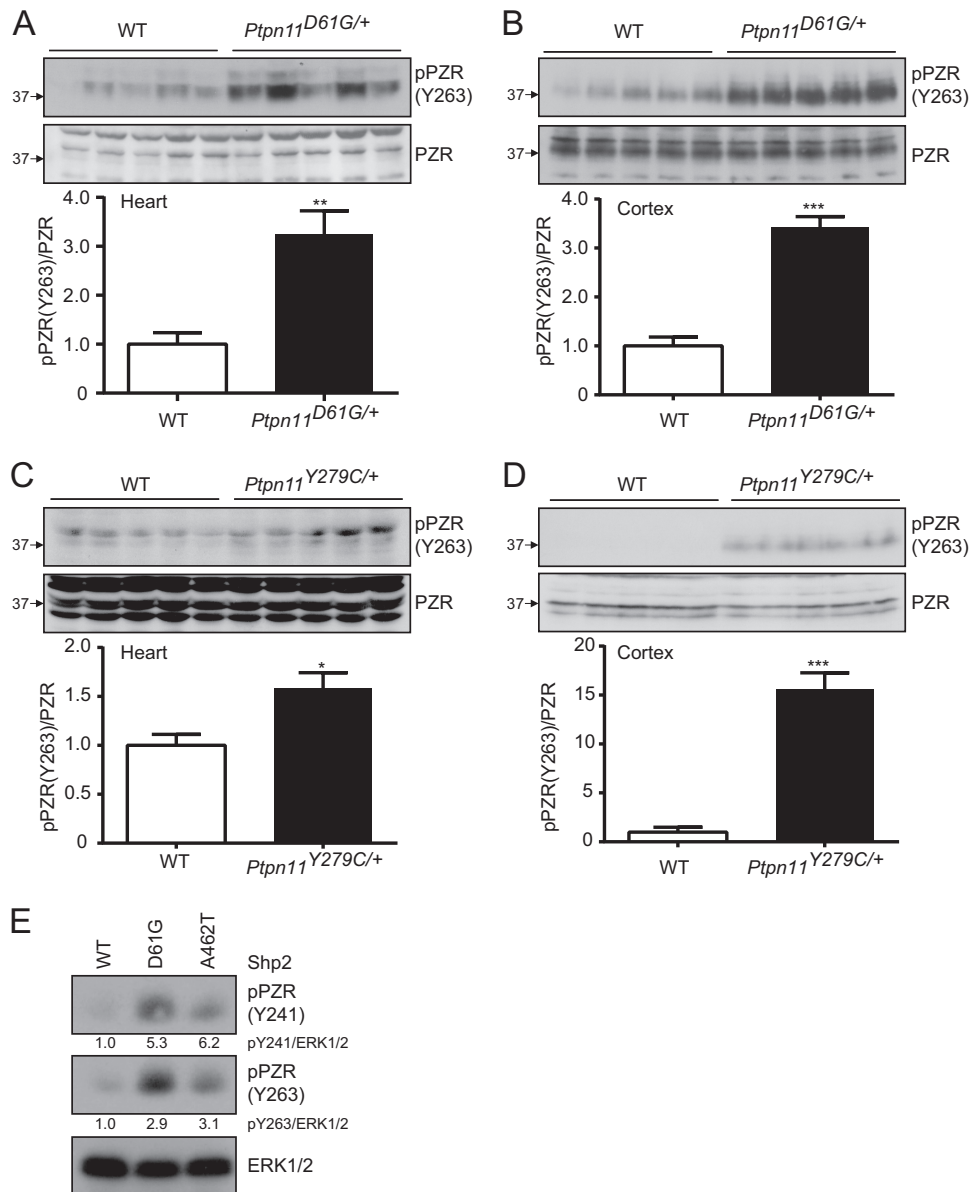


FIG 7 PZR tyrosyl phosphorylation in *Ptpn11*^{D61G/+} and *Ptpn11*^{Y279C/+} mice and zebrafish expressing D61G or A462T Shp2. The heart (A and C) and the cortex (B and D) were isolated from 5-week-old WT and *Ptpn11*^{D61G/+} mice (A and B) or 8-week-old WT and *Ptpn11*^{Y279C/+} mice (C and D). Tissue lysates were immunoblotted with pPZR(Y263) and total PZR antibodies. Phosphorylation of tyrosine 264 in PZR represents $n = 5$ per genotype. All data are means \pm standard errors of the means (SEM). *, $P < 0.05$; **, $P < 0.01$; ***, $P < 0.001$. (E) Lysates prepared from zebrafish embryos expressing either wild-type, D61G, or A462T Shp2 were immunoblotted with anti-PZR pY241 and anti-PZR pY263 antibodies. Relative quantitation is shown below, and ERK1/2 expression was used as a loading control.

defects (Fig. 5). However, partial knockdown of PZR and Shp2 together resulted in severe developmental defects at 4 dpf (Fig. 5). The embryos were scored in three categories (wild type [WT], phenotype, and severe), and it was evident that cknockdown of Shp2 and PZR greatly enhanced the percentage of embryos displaying a severe defect phenotype (Fig. 5). PZR knockdown also induced wider-set eyes, reminiscent of the phenotype that we and others reported in Shp2 knockdowns (11, 44). Together, these results are consistent with the notion that PZR and Shp2 function in a conserved signaling pathway in zebrafish.

NS- and LS-associated Shp2 mutants induce PZR Y241 and Y263 hyper-tyrosyl phosphorylation. We investigated the char-

acteristics of PZR hyper-tyrosyl phosphorylation in further detail. To accomplish this, antibodies against tyrosyl-phosphorylated PZR at Y241 (pY241-PZR) and Y263 (pY263-PZR) were generated. When cells were cotransfected with PZR, along with an activating mutant of Shp2 (Shp2^{E76A}) that induces PZR hyper-tyrosyl phosphorylation (25), both anti-pY241 and anti-pY263-PZR antibodies recognized tyrosyl-phosphorylated PZR (Fig. 6A). When Y263 in PZR was mutated to F263, neither anti-pY241 nor anti-pY263-PZR antibodies detected tyrosyl-phosphorylated PZR upon coexpression of Shp2^{E76A} (Fig. 6A). Similarly, mutation of Y241 to F241 in PZR also resulted in the failure of both anti-pY241 and anti-pY263-PZR antibodies to detect tyrosyl-phosphorylated

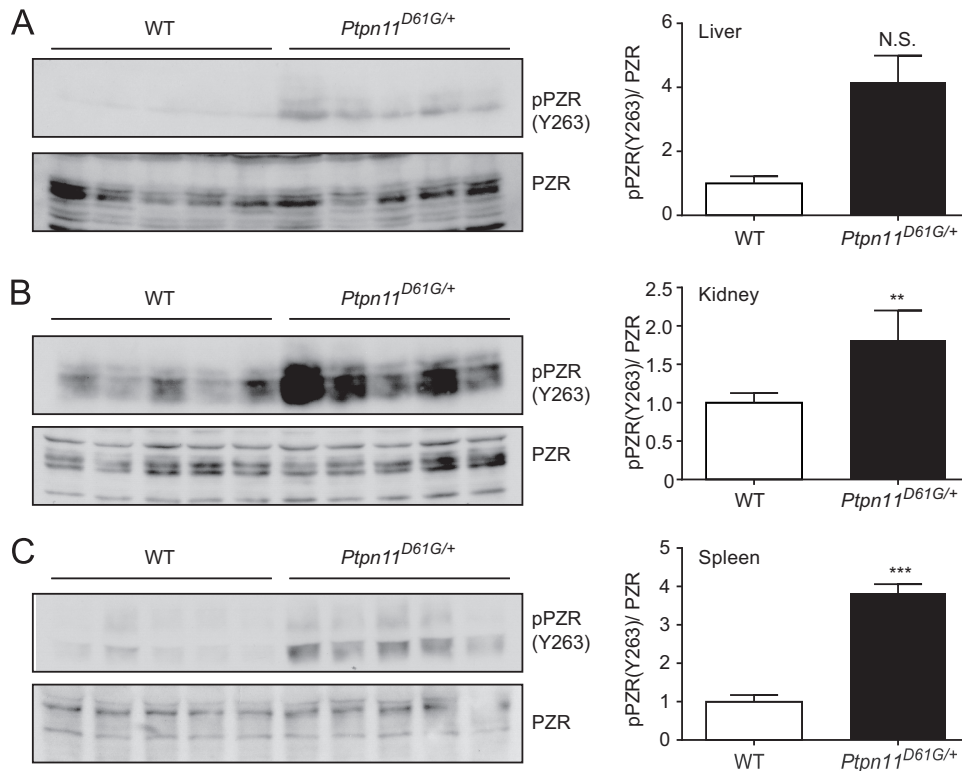


FIG 8 PZR tyrosyl phosphorylation in *Ptpn11*^{D61G/+} mice. Liver (A), kidney (B), and spleen (C) were isolated from 5-week-old wild-type and *Ptpn11*^{D61G/+} mice. Tissue lysates were immunoblotted with anti-pPZR(Y263) and -total PZR antibodies. Densitometric analysis of the phosphorylation levels of tyrosine 263 in PZR was performed, and the results represent the means \pm SEM from 5 mice per genotype. **, $P < 0.01$; ***, $P < 0.001$ (WT versus NS).

PZR (Fig. 6A). The explanation for these results is that Y241 is required for Y263 phosphorylation, and conversely, Y263 is required for Y241 phosphorylation. Similar observations have been made by others (21, 45). Importantly, mutation of Y241 and Y263 to nonphosphorylatable residues abolished the immunoreactivity of both phospho-specific PZR antibodies (Fig. 6A). These antibodies also recognized Y241 and Y263 in zebrafish PZR (Fig. 6B).

We tested whether activating Shp2 mutants induced either Y241 PZR or Y263 PZR tyrosyl phosphorylation in other cell types. To this end, the wild type and activating Shp2^{E76A} mutants were introduced into human umbilical vein endothelial cells (HUVECs). These results indicated that pY241-PZR and pY263-PZR antibodies recognized endogenous tyrosyl-phosphorylated PZR at Y241 and Y263, respectively (Fig. 6C). The LS mutants from humans and zebrafish when expressed in 293 cells were capable of inducing PZR hyper-tyrosyl phosphorylation at both Y241 and Y263 (Fig. 6D and E). As reported previously (25), increased zebrafish PZR tyrosyl phosphorylation correlated with enhanced PZR/Shp2 binding (Fig. 6E). Hence, both NS and LS mutations in humans and zebrafish enhance PZR tyrosyl phosphorylation.

PZR hyper-tyrosyl phosphorylation in NS and LS mice. We determined whether PZR was hyper-tyrosyl phosphorylated in NS mice. Hearts isolated from 8-week-old wild-type and *Ptpn11*^{D61G/+} mice showed a significant increase in pY263-PZR tyrosyl phosphorylation compared with wild-type controls (Fig. 7A). In addition, PZR hyper-tyrosyl phosphorylation was observed in the cortex of *Ptpn11*^{D61G/+} mice (Fig. 7B), as well as in the kidney, liver, and spleen of these mice (Fig. 8A to C).

Given that in cultured cells LS induces PZR hyper-tyrosyl phosphorylation (Fig. 6D and E), we tested whether PZR is hyper-tyrosyl phosphorylated using *Ptpn11*^{Y279C/+} knock-in mutant mice, which represented a human LS mutant (46). Hearts from *Ptpn11*^{Y279C/+} mice were isolated, and although to a much lesser extent than *Ptpn11*^{D61G/+} mice, PZR was hyper-tyrosyl phosphorylated on Y263 (Fig. 7C). In addition, PZR was robustly hyper-tyrosyl phosphorylated in the cortex of *Ptpn11*^{Y279C/+} mice (Fig. 7D). In agreement with these data, we also observed that when zebrafish embryos were injected to express either the NS or LS mutants, PZR was also hyper-tyrosyl phosphorylated at Y241 and Y263 (Fig. 7E). No apparent differences were observed in the basal levels of Shp2, phospho-ERK1/2, or phospho-Akt between NS or LS mice (Fig. 9A to D). Collectively, these results show that both NS and LS mutants induce PZR hyper-tyrosyl phosphorylation within the ITIM Shp2 binding motif of PZR in mice and zebrafish.

NS and LS mutants induce PZR hyper-tyrosyl phosphorylation by enhancing the Src/Shp2/PZR complex. In order to investigate the mechanisms underlying how both NS and LS mutants induce PZR hyper-tyrosyl phosphorylation, we examined the dependency of NS and LS mutants to induce PZR hyper-tyrosyl phosphorylation through the SFKs. ITIMs serve as potent Src family kinase (SFK) substrates, and SFKs phosphorylate ITIMs within PZR (47). Pharmacological inhibition of the SFKs by SU6656 impaired both NS- and LS-induced PZR hyper-tyrosyl phosphorylation at pY241 and pY263 (Fig. 10A). Similar results were also observed with the activated E76A mutant with both SU6656 and the broader-specificity tyrosine kinase inhibitor PP2 (Fig. 10B).

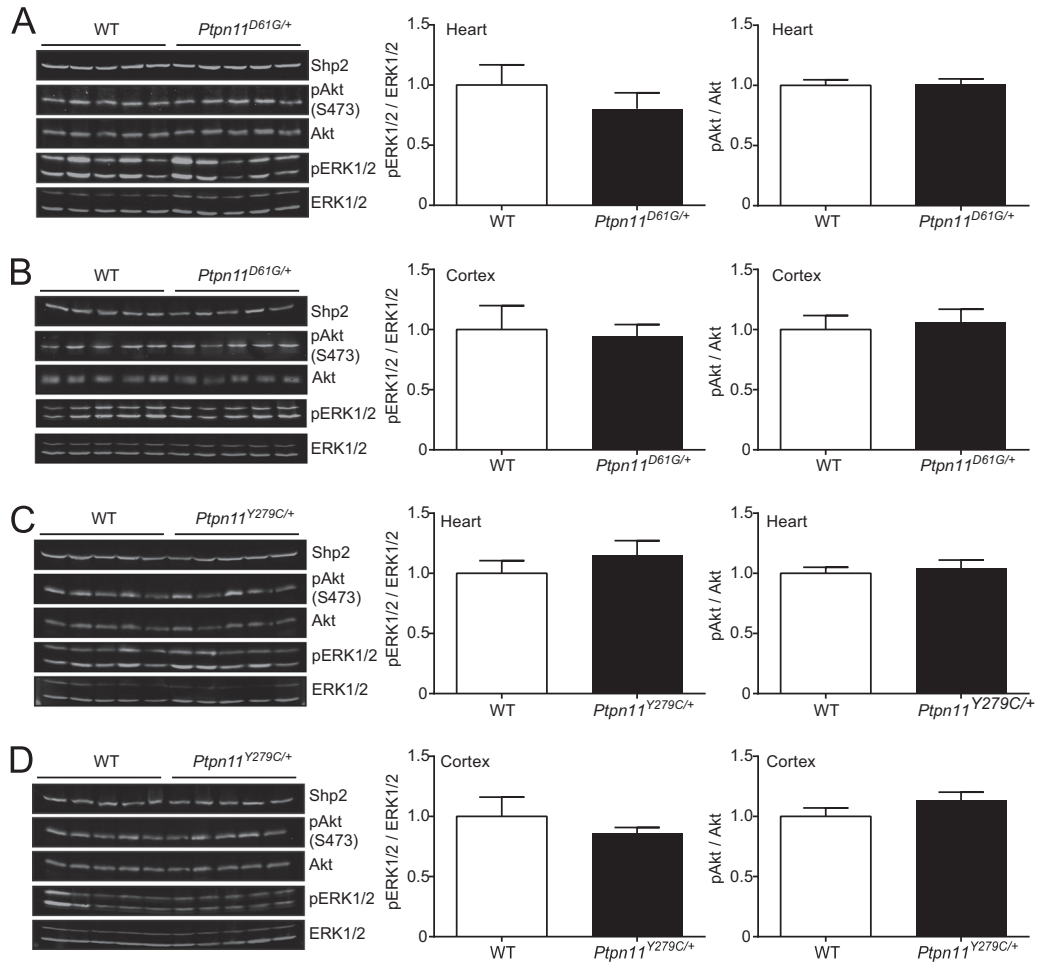


FIG 9 ERK and Akt phosphorylation in *Ptpn11^{D61G/+}* and *Ptpn11^{Y279C/+}* mice. The heart (A and C) and the cortex (B and D) were isolated from 5-week-old wild-type and *Ptpn11^{D61G/+}* mice (A and B) or 8-week-old wild-type and *Ptpn11^{Y279C/+}* mice (C and D). Tissue lysates were subjected to immunoblotting with anti-Shp2, -pERK1/2, -total ERK1/2, -pAkt, and -Akt antibodies. The results represent densitometric analyses of the means \pm SEM for pERK1/2 and pAkt from 5 mice per genotype.

Next, we determined the ability of the activating Shp2 mutant to induce PZR hyper-tyrosyl phosphorylation in fibroblasts lacking the expression of Src/Yes/Fyn (SYF cells). Here, we found that an activating Shp2 mutant failed to induce PZR hyper-tyrosyl phosphorylation at Y241 and Y263 (Fig. 11A). Consistent with this, a kinase-dead mutant of c-Src blocked the ability of the activated Shp2 mutant to induce PZR hyper-tyrosyl phosphorylation at these specific sites (Fig. 11B). Both human and zebrafish PZR served as c-Src substrates *in vitro* (Fig. 11C and D), and coexpression of a constitutively activated mutant of c-Src promoted tyrosyl phosphorylation of zebrafish PZR in cells (Fig. 11E). Hence, c-Src phosphorylates human and zebrafish PZR at the Shp2 binding sites, demonstrating that the SFKs likely mediate PZR hyper-tyrosyl phosphorylation.

It has been previously suggested that the “open” conformations of both NS and LS mutants exhibit properties that increase their propensity to interact with other signaling proteins. Based upon our observations that SFKs may play a role, we tested whether the SFKs are NS and/or LS binding targets. To test this, c-Src was immunoprecipitated from cells expressing either wild-type Shp2 or NS or LS mutants, and these immune complexes

were immunoblotted to detect the presence of Shp2. We found that in both NS- and LS-expressing cells, the amount of NS/LS Shp2 present in c-Src complexes was significantly greater than that in the wild-type Shp2-expressing cells (Fig. 12A).

To determine whether Src is present in PZR complexes and whether this is enhanced by the “open” conformation of mutated Shp2, we immunoprecipitated Src and assessed the extent of PZR interactions. We found that when Src was immunoprecipitated, PZR and Shp2 were present in the complex (Fig. 12B). However, Src failed to coimmunoprecipitate with the form of PZR that was mutated in both of the ITIMs but still exhibited enhanced Shp2 binding to the “open” conformation Shp2 mutants (Fig. 12B). Wild-type PZR, as expected, was found to exist in a complex with Shp2, and this was further enhanced when either the activating or LS Shp2-containing mutation was expressed (Fig. 12B). In contrast, double-ITIM-containing mutant PZR failed to form a complex (Fig. 12B). These results suggest that the “open” conformation of Shp2 mutants exhibits an increased propensity to bind c-Src and that the likely explanation for PZR-induced hyper-tyrosyl phosphorylation is causally related to the ability of Src to increase its proximity to PZR through Shp2 binding.

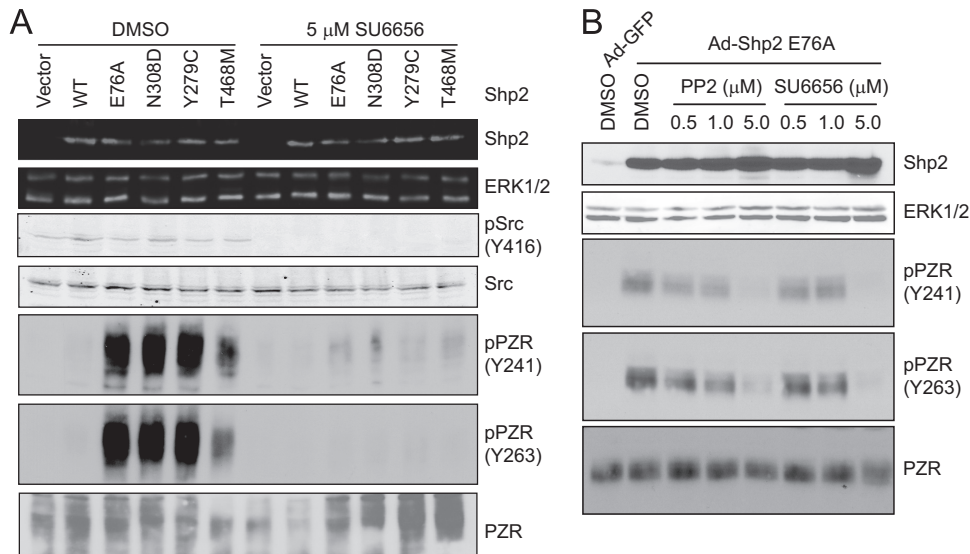


FIG 10 Effect of Src family kinases on PZR Y241 and Y263 phosphorylation. (A) HEK-293 cells were transiently transfected with the indicated Shp2 mutants and treated with either dimethyl sulfoxide (DMSO) as a control or 5 μ M SU6656. (B) NIH 3T3 cells were infected with the adenoviruses expressing either GFP as a control or a constitutively active Shp2^{E76A}, in the presence of DMSO, PP2, or SU6656 at the indicated concentration. Cell lysates were immunoblotted with anti-Shp2, pSrc(Y416), Src, pPZR(Y241 or Y263), and total PZR antibodies. ERK1/2 was used as a loading control.

Convergence and extension defects induced by NS and LS are recapitulated by PZR in a phosphotyrosyl-dependent manner.

The similarities between the Shp2 (42) and PZR morphant phenotypes (Fig. 3 and 5) indicate common defects during development. Previous results have shown that Shp2 knockdown and NS and LS *PTPN11* mutant overexpression lead to convergence and extension (C/E) cell movement defects during gastrulation, resulting in shorter embryos with craniofacial defects and cardiac edema (11). To test whether PZR knockdown also induces C/E defects, embryos were injected with PZR, Shp2, or control MO, or LS mRNA as a positive control. Embryos were fixed at the 8- to 10-somite stage, subjected to *in situ* hybridization, and stained for *krox20* and *myoD*, markers for rhombomeres 3 and 5 and the somites, respectively. Loss of PZR led to shorter and wider embryos than controls at the same stage, and these phenotypes were similar to Shp2 knockdown and LS-Shp2-injected embryos (Fig. 13A). These results indicated that PZR is essential for C/E cell movements, analogous to those of both NS and LS mutants during zebrafish gastrulation.

To assess whether PZR tyrosyl phosphorylation sites were important for C/E phenotypes, we overexpressed wild-type PZR and PZR tyrosyl phosphorylation site-deficient mutants and performed *in situ* hybridization at the 8- to 10-somite stage using *krox20* and *myoD* markers. Overexpression of wild-type PZR resulted in shorter and wider embryos (Fig. 13B). When mRNA encoding double ITIM tyrosine-to-phenylalanine mutants (Y241F and Y263F [2YF]) and as a control mRNA encoding GFP were injected into zebrafish embryos, the C/E phenotype was inhibited (Fig. 13B). As expected, PZR tyrosyl phosphorylation and Shp2 binding to zebrafish PZR are inhibited in the double ITIM Y241F/Y263F mutant (Fig. 13C). These data indicate that tyrosyl phosphorylation of the ITIMs are required for PZR signaling for the promotion of the C/E phenotype during early development in zebrafish.

DISCUSSION

Here, we identified using nonbiased proteomic approaches PZR as a major hyper-tyrosyl-phosphorylated protein in both NS and LS models of mice and zebrafish. Remarkably, disruption of PZR function resulted in phenotypes similar to that observed in NS or LS mutant-expressing zebrafish. Mechanistically, NS and LS mutants induce PZR tyrosyl phosphorylation in an Src-dependent manner, and these mutants acquire an enhanced Src interaction compared with wild-type Shp2. PZR is required for zebrafish gastrulation, and tyrosyl phosphorylation is necessary to promote convergence and extension movements. Thus, NS and LS mutants promiscuously promote PZR hyper-tyrosyl phosphorylation, leading to dysfunctional gastrulation. Collectively, these results suggest that PZR is a novel target for both NS- and LS-associated Shp2 mutants.

The extracellular matrix serves to integrate dynamically processes that govern cell fate, tissue maintenance, and homeostasis to outcomes that dictate organ architecture (48). Growth factor receptors, chemokines, and G-protein-coupled receptors are either directly or indirectly influenced by the extracellular matrix (ECM) to control cell proliferation, differentiation, and cell survival. The “RASopathies” represent mutated components of the SOS/Ras/Raf/Erk pathway, and there has been much focus on the role this cascade plays in NS and LS as it relates to cell proliferation and cell survival (10). PZR has been shown to function in the control of cell adhesion and migration (24, 25, 45, 47, 49). Therefore, our findings imply that aberrant cell migration and adhesion likely play important roles in the pathogenesis of both NS and LS. The development of PZR mutant mice will be necessary to test these conclusions more comprehensively.

Germ line mutations in *Ptpn11* that result in either increased or decreased protein tyrosine phosphatase activity lead to developmental defects in zebrafish, mice, and humans. Our findings that PZR is a target for *Ptpn11* mutations that exhibit either increased

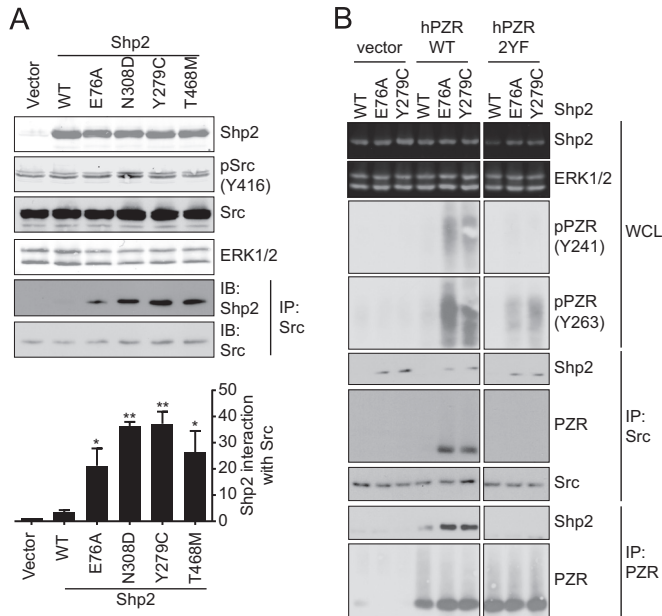


FIG 12 Enhanced Src complex formation with NS/LS-associated Shp2 mutants. (A) HEK-293 cells were transiently transfected either with the Shp2 WT and the indicated Shp2 mutants. Cell lysates were immunoprecipitated (IP) with anti-c-Src antibodies, and immune complexes were immunoblotted (IB) with anti-Shp2 and -Src antibodies. The graph represents the means \pm SEM of the densitometric analysis from three independent experiments. Statistical significance was derived using a Dunnett's test comparing Shp2 mutants with the WT. *, $P < 0.05$; **, $P < 0.01$. (B) HEK-293 cells were cotransfected with the Shp2 WT or E76A or Y279C mutant and either empty vector (vector), WT human PZR, or the PZR 2YF mutant. Cell lysates were immunoblotted with anti-pPZR (Y241 or Y263) or -Shp2 antibodies. ERK1/2 was used as a loading control. Immune complexes were immunoblotted with anti-Src, -Shp2, and -PZR antibodies.

(11). These results suggest a tight balance and interplay exist between PZR and Shp2 signaling, consistent with the biochemical evidence demonstrating that Shp2 binds directly to PZR within its ITIMs (11). Collectively, these observations argue that PZR-mediated tyrosyl phosphorylation in zebrafish and mice serves as a mechanism to promote NS and LS signaling.

What are the consequences of increased PZR tyrosyl phosphorylation? PZR acts as an adhesion-responsive glycoprotein where, upon engagement to the extracellular matrix, it becomes rapidly tyrosyl phosphorylated within its ITIMs. Upon tyrosyl phosphorylation, Shp2 is recruited to PZR, and it has been shown that this event is responsible for promoting the promigratory and cell adhesive effects in a variety of cell types (24, 25, 45, 47, 49). Given the importance of cell migration and cell adhesion in developmental processes, such as gastrulation, it is conceivable that aberrant PZR tyrosyl phosphorylation induced by both NS and LS mutants disrupts this process. In mice, PZR is expressed during early development, and we have demonstrated that PZR is hyper-tyrosyl phosphorylated in the developing embryo of *Ptpn11*^{D61G/+} mice (25). These observations support the notion that altered PZR tyrosyl phosphorylation and hence downstream signaling are associated with developmental defects. The significance of PZR tyrosyl phosphorylation was demonstrated in experiments in which overexpression of the ITIM mutants of PZR failed to induce gastrulation defects. These results define PZR tyrosyl phosphorylation as critical for development.

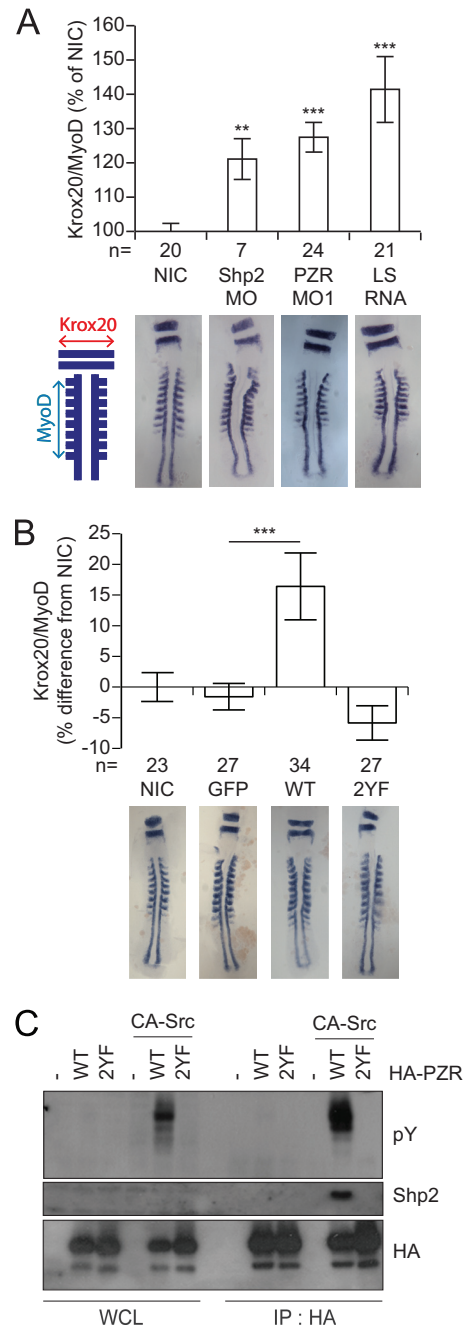


FIG 13 PZR tyrosyl phosphorylation is necessary for the zebrafish convergence and extension phenotype. (A) Embryos were injected with Shp2 MO, PZR MO, or LS mRNA at the 1-cell stage and fixed at the 8- to 10-somite stage. *In situ* hybridization was performed using *krox20* and *myoD* staining for rhombomeres 3 and 5 and somites, respectively. Quantification of the width of the rhombomeres (red) and the length of the first 8 somites (light blue) is shown schematically. *krox20/myoD* ratios are plotted compared to those of noninjected controls (NIC). Data represent means \pm SEM. **, $P < 0.01$; ***, $P < 0.001$. (B) Embryos were injected at the 1-cell stage with mRNA encoding GFP, wild-type (WT) PZR, or PZR with the indicated mutations. Ratios of *krox20* to *myoD* were calculated and compared to those of NIC. All data represent means \pm SEM. ***, $P < 0.001$. (C) HEK-293 cells were cotransfected with either the HA-tagged zebrafish PZR WT or 2YF mutant and constitutively active Src. Cell lysates were immunoprecipitated with HA antibody and blotted with anti-pY, -Shp2, and -HA antibodies.

A provocative finding from our study is that these results implicate the actions of a tyrosine kinase that promotes PZR tyrosyl phosphorylation by both NS and LS mutants. The observation that PZR is hyper-tyrosyl phosphorylated in both NS and LS most likely indicates that the ability of the kinase to phosphorylate PZR occurs in an Shp2 catalytically independent manner. We had shown previously that enhanced PZR tyrosyl phosphorylation caused by NS mutants does not occur as a result of SH2 domain protection (25). Rather, the data here support an Src family kinase as responsible for NS- and LS-induced PZR hyper-tyrosyl phosphorylation. Previous work had initially suggested a lack of SFK involvement in NS-mediated PZR hyper-tyrosyl phosphorylation (25). In the study by Eminaga et al., we immunoprecipitated Shp2 and analyzed tyrosyl phosphorylation of Shp2-associated proteins. The Shp2-associated tyrosyl-phosphorylated complex that migrated with a molecular mass of ~40 kDa was found to contain at least PZR. It is likely that in this p40 complex, “site-specific” PZR tyrosyl phosphorylation was obscured by other comigrating tyrosyl-phosphorylated proteins. Whereas, in the experiments presented here, PZR tyrosyl phosphorylation is assessed directly using site-specific phospho antibodies.

We found that both NS and LS mutants contain increased levels of c-Src complexes compared with wild-type Shp2. In addition, we showed increased PZR in Src complexes from activating and LS-associated Shp2 mutants, and this was abolished in cells expressing the PZR tyrosyl phosphorylation-deficient mutant. The nature of this increased association with c-Src correlates with the common underlying property that both NS and LS mutants exhibit an “open” conformation (19, 50). Other groups have suggested that the “open” conformation of NS and LS may represent an important molecular mechanism for the pathogenesis of these mutant forms of Shp2 (19, 20, 44, 50). The open conformation of NS and LS mutants exposes the PTP and SH2 domains; presumably, this presents binding surfaces for Src that are otherwise inaccessible. Indeed, it has been shown previously that Shp2 binds to Src through its SH3 domains (51, 52). Our findings support this observation and extend it by providing a mechanism that reconciles the behavior of both NS and LS in their capacity to promote similar phenotypic outcomes.

The results from our proteomic screen are consistent with activation of an SFK-mediated pathway as we identified the Src substrate, focal adhesion kinase (FAK), and PECAM as hyper-tyrosyl phosphorylated in the hearts of NS mice. JNK was increased in its level of tyrosyl phosphorylation at one of its activating phosphorylation sites in NS hearts. Interestingly, Marin et al. showed that JNK and FAK were hyper-tyrosyl phosphorylated in LS mice, suggesting a catalytic-independent mechanism for the activation of these molecules through the effects of enhanced Src function (46). Whether the PZR/Shp2/Src pathway accounts for the entirety of either the NS- or LS-like phenotype will need to be determined. However, Jopling et al. have shown that Shp2 lies upstream of the SFKs in zebrafish development, and the Shp2/SFK pathway is required for convergence and extension cell movements (11). An integrated interpretation of our results supports a model in which we invoke the actions of enhanced Src-mediated PZR tyrosyl phosphorylation that results in altered development. An important aspect of Shp2-mediated signaling is that it is required to be appropriately localized to its upstream target. Disruption of the SH2 domains of Shp2 results in the abrogation of its ability to signal (1). Therefore, enhanced PZR tyrosyl phosphorylation re-

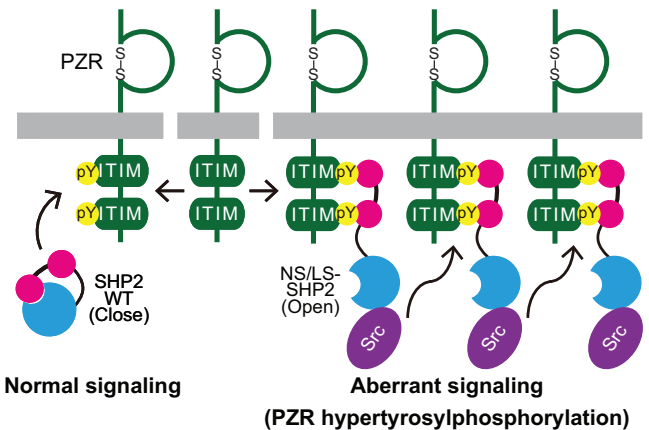


FIG 14 Model for the effects of NS and LS mutants on PZR tyrosyl phosphorylation. See the text for details.

sults in increased recruitment of Shp2 to PZR to promote further PZR tyrosyl phosphorylation and presumably other Src substrates that are in close proximity (Fig. 14). It should also be noted that Src couples to Ras and in some cases does so through Shp2 (53). It is formally possible that both NS and LS engage Ras via this mechanism. However, the contribution of Ras signaling specifically for the manifestation of NS- or LS-related pathologies has yet to be determined. Collectively, these observations go some way toward providing an explanation as to how both the NS and LS mutants, which have enhanced and inactive PTP activities, respectively, result in overlapping phenotypes.

In summary, we have identified PZR as a proximal target of both NS and LS mutants. PZR functions to regulate cell adhesion and cell migration. Therefore, in NS and LS the augmentation of PZR's interaction with Shp2 when it is hyper-tyrosyl phosphorylated presumably disrupts key developmental events that rely on the appropriate delivery of migratory cues. This mechanism occurs through enhanced binding of NS and LS mutants to Src. The implications of our findings clinically are that they suggest that the magnitude of PZR tyrosyl phosphorylation may reflect the “openness” of *Ptpn11* mutants and hence the severity of NS- and LS-related diseases. As such, it would be instructive to assess the clinical genotype-phenotype relationship in the context of PZR tyrosyl phosphorylation in NS and LS patients.

ACKNOWLEDGMENTS

This work was supported by NIH grant R01 GM099801 (A.M.B.) and in part by a grant from the Research Council for Earth and Life Sciences (ALW 819.02.021) with financial aid from the Netherlands Organization for Scientific Research (NWO) (to J.D.H.).

REFERENCES

1. Neel BG, Guo H, Pao L. 2009. SH2 domain-containing protein tyrosine phosphatases, p 707–728. In Bradshaw RA, Dennis EA (ed), Handbook in cell signaling, 2nd ed, vol 2. Elsevier, San Diego, CA.
2. Hof P, Pluskey S, Dhe-Pagannon S, Eck MJ, Shoelson SE. 1998. Crystal structure of the tyrosine phosphatase SHP-2. *Cell* 92:441–450. [http://dx.doi.org/10.1016/S0092-8674\(00\)80938-1](http://dx.doi.org/10.1016/S0092-8674(00)80938-1).
3. Mohi MG, Williams IR, Dearolf CR, Chan G, Kutok JL, Cohen S, Morgan K, Boulton C, Shigematsu H, Keilhack H, Akashi K, Gilliland DG, Neel BG. 2005. Prognostic, therapeutic, and mechanistic implications of a mouse model of leukemia evoked by Shp2 (PTPN11) mutations. *Cancer Cell* 7:179–191. <http://dx.doi.org/10.1016/j.ccr.2005.01.010>.

4. Tiganis T, Bennett AM. 2007. Protein tyrosine phosphatase function: the substrate perspective. *Biochem. J.* 402:1–15. <http://dx.doi.org/10.1042/BJ20061548>.
5. Saxton TM, Henkemeyer M, Gasca S, Shen R, Rossi DJ, Shalaby F, Feng GS, Pawson T. 1997. Abnormal mesoderm patterning in mouse embryos mutant for the SH2 tyrosine phosphatase Shp-2. *EMBO J.* 16:2352–2364. <http://dx.doi.org/10.1093/emboj/16.9.2352>.
6. Yang W, Klamann LD, Chen B, Araki T, Harada H, Thomas SM, George EL, Neel BG. 2006. A Shp2/SFK/Ras/Erk signaling pathway controls trophoblast stem cell survival. *Dev. Cell* 10:317–327. <http://dx.doi.org/10.1016/j.devcel.2006.01.002>.
7. Perkins LA, Larsen I, Perrimon N. 1992. *corkscrew* encodes a putative protein tyrosine phosphatase that functions to transduce the terminal signal from the receptor tyrosine kinase torso. *Cell* 70:225–236. [http://dx.doi.org/10.1016/0092-8674\(92\)90098-W](http://dx.doi.org/10.1016/0092-8674(92)90098-W).
8. Neel BG, Gu H, Pao L. 2003. The ‘Shp’ing news: SH2 domain-containing tyrosine phosphatases in cell signaling. *Trends Biochem. Sci.* 28:284–293. [http://dx.doi.org/10.1016/S0968-0004\(03\)00091-4](http://dx.doi.org/10.1016/S0968-0004(03)00091-4).
9. Tartaglia M, Mehler EL, Goldberg R, Zampino G, Brunner HG, Kremer H, van der Burgt I, Crosby AH, Ion A, Jeffery S, Kalidas K, Patton MA, Kucherlapati RS, Gelb BD. 2001. Mutations in PTPN11, encoding the protein tyrosine phosphatase SHP-2, cause Noonan syndrome. *Nat. Genet.* 29:465–468. <http://dx.doi.org/10.1038/ng772>.
10. Tartaglia M, Gelb BD. 2005. Noonan syndrome and related disorders: genetics and pathogenesis. *Annu. Rev. Genomics Hum. Genet.* 6:45–68. <http://dx.doi.org/10.1146/annurev.genom.6.080604.162305>.
11. Jopling C, van Geemen D, den Hertog J. 2007. Shp2 knockdown and Noonan/LEOPARD mutant Shp2-induced gastrulation defects. *PLoS Genet.* 3:e225. <http://dx.doi.org/10.1371/journal.pgen.0030225>.
12. Runtuwene V, van Eekelen M, Overvoorde J, Rehmann H, Yntema HG, Nillesen WM, van Haeringen A, van der Burgt I, Burgering B, den Hertog J. 2011. Noonan syndrome gain-of-function mutations in NRAS cause zebrafish gastrulation defects. *Dis. Model Mech.* 4:393–399. <http://dx.doi.org/10.1242/dmm.007112>.
13. Tidyman WE, Rauen KA. 2008. Noonan, Costello and cardio-facio-cutaneous syndromes: dysregulation of the Ras-MAPK pathway. *Expert Rev. Mol. Med.* 10:e37. <http://dx.doi.org/10.1017/S1462399408000902>.
14. Gelb BD, Tartaglia M. 2011. RAS signaling pathway mutations and hypertrophic cardiomyopathy: getting into and out of the thick of it. *J. Clin. Invest.* 121:844–847. <http://dx.doi.org/10.1172/JCI46399>.
15. Kontaridis MI, Swanson KD, David FS, Barford D, Neel BG. 2006. PTPN11 (Shp2) mutations in LEOPARD syndrome have dominant negative, not activating, effects. *J. Biol. Chem.* 281:6785–6792. <http://dx.doi.org/10.1074/jbc.M513068200>.
16. Tartaglia M, Martinelli S, Stella L, Bocchinfuso G, Flex E, Cordeddu V, Zampino G, Burgt IV, Palleschi A, Petrucci TC, Sorcini M, Schoch C, Foa R, Emanuel PD, Gelb BD. 2006. Diversity and functional consequences of germline and somatic PTPN11 mutations in human disease. *Am. J. Hum. Genet.* 78:279–290. <http://dx.doi.org/10.1086/499925>.
17. Hanna N, Montagner A, Lee WH, Miteva M, Vidal M, Vidaud M, Parfait B, Raynal P. 2006. Reduced phosphatase activity of SHP-2 in LEOPARD syndrome: consequences for PI3K binding on Gab1. *FEBS Lett.* 580:2477–2482. <http://dx.doi.org/10.1016/j.febslet.2006.03.088>.
18. Gelb BD, Tartaglia M. 2006. Noonan syndrome and related disorders: dysregulated RAS-mitogen activated protein kinase signal transduction. *Hum. Mol. Genet.* 15(Suppl 2):R220–R226. <http://dx.doi.org/10.1093/hmg/ddl197>.
19. Yu ZH, Xu J, Walls CD, Chen L, Zhang S, Zhang R, Wu L, Wang L, Liu S, Zhang ZY. 2013. Structural and mechanistic insights into LEOPARD syndrome-associated SHP2 mutations. *J. Biol. Chem.* 288:10472–10482. <http://dx.doi.org/10.1074/jbc.M113.450023>.
20. Qiu W, Wang X, Romanov V, Hutchinson A, Lin A, Ruzanov M, Battaile KP, Pai EF, Neel BG, Chirgadze NY. 2014. Structural insights into Noonan/LEOPARD syndrome-related mutants of protein-tyrosine phosphatase SHP2 (PTPN11). *BMC Struct. Biol.* 14:10. <http://dx.doi.org/10.1186/1472-6807-14-10>.
21. Zhao R, Zhao ZJ. 2000. Dissecting the interaction of SHP-2 with PZR, an immunoglobulin family protein containing immunoreceptor tyrosine-based inhibitory motifs. *J. Biol. Chem.* 275:5453–5459. <http://dx.doi.org/10.1074/jbc.275.8.5453>.
22. Zhao R, Zhao ZJ. 2003. Identification of a variant form of PZR lacking immunoreceptor tyrosine-based inhibitory motifs. *Biochem. Biophys. Res. Commun.* 303:1028–1033. [http://dx.doi.org/10.1016/S0006-291X\(03\)00484-4](http://dx.doi.org/10.1016/S0006-291X(03)00484-4).
23. Zhao ZJ, Zhao R. 1998. Purification and cloning of PZR, a binding protein and putative physiological substrate of tyrosine phosphatase SHP-2. *J. Biol. Chem.* 273:29367–29372. <http://dx.doi.org/10.1074/jbc.273.45.29367>.
24. Roubelakis MG, Martin-Rendon E, Tsaknakis G, Stavropoulos A, Watt SM. 2007. The murine ortholog of the SHP-2 binding molecule, PZR accelerates cell migration on fibronectin and is expressed in early embryo formation. *J. Cell. Biochem.* 102:955–969. <http://dx.doi.org/10.1002/jcb.21334>.
25. Eminaga S, Bennett AM. 2008. Noonan syndrome-associated SHP-2/PTPN11 mutants enhance SIRPalpha and PZR tyrosyl phosphorylation and promote adhesion-mediated Erk activation. *J. Biol. Chem.* 283:15328–15338. <http://dx.doi.org/10.1074/jbc.M801382200>.
26. Saxton TM, Pawson T. 1999. Morphogenetic movements at gastrulation require the SH2 tyrosine phosphatase Shp2. *Proc. Natl. Acad. Sci. U. S. A.* 96:3790–3795. <http://dx.doi.org/10.1073/pnas.96.7.3790>.
27. van der Wijk T, Blanchetot C, Overvoorde J, den Hertog J. 2003. Redox-regulated rotational coupling of receptor protein-tyrosine phosphatase alpha dimers. *J. Biol. Chem.* 278:13968–13974. <http://dx.doi.org/10.1074/jbc.M300632200>.
28. Kontaridis MI, Eminaga S, Fornaro M, Zito CI, Sordella R, Settleman J, Bennett AM. 2004. SHP-2 positively regulates myogenesis by coupling to the Rho GTPase signaling pathway. *Mol. Cell. Biol.* 24:5340–5352. <http://dx.doi.org/10.1128/MCB.24.12.5340-5352.2004>.
29. Fornaro M, Burch PM, Yang W, Zhang L, Hamilton CE, Kim JH, Neel BG, Bennett AM. 2006. SHP-2 activates signaling of the nuclear factor of activated T cells to promote skeletal muscle growth. *J. Cell Biol.* 175:87–97. <http://dx.doi.org/10.1083/jcb.200602029>.
30. Araki T, Mohi MG, Ismat FA, Bronson RT, Williams IR, Kutok JL, Yang W, Pao LI, Gilliland DG, Epstein JA, Neel BG. 2004. Mouse model of Noonan syndrome reveals cell type- and gene dosage-dependent effects of Ptpn11 mutation. *Nat. Med.* 10:849–857. <http://dx.doi.org/10.1038/nm1084>.
31. Westerfield M. 1995. The zebrafish book. A guide for the laboratory use of zebrafish (*Danio rerio*), 3rd ed. University of Oregon Press, Eugene, OR.
32. Thisse C, Thisse B, Schilling TF, Postlethwait JH. 1993. Structure of the zebrafish snail1 gene and its expression in wild-type, spadetail and no tail mutant embryos. *Development* 119:1203–1215.
33. van Eekelen M, Runtuwene V, Overvoorde J, den Hertog J. 2010. RPTPalpa and PTPepsilon signaling via Fyn/Yes and RhoA is essential for zebrafish convergence and extension cell movements during gastrulation. *Dev. Biol.* 340:626–639. <http://dx.doi.org/10.1016/j.ydbio.2010.02.026>.
34. Rikova K, Guo A, Zeng Q, Possemato A, Yu J, Haack H, Nardone J, Lee K, Reeves C, Li Y, Hu Y, Tan Z, Stokes M, Sullivan L, Mitchell J, Wetzel R, Macneill J, Ren JM, Yuan J, Bakalarski CE, Villen J, Kornhauser JM, Smith B, Li D, Zhou X, Gygi SP, Gu TL, Polakiewicz RD, Rush J, Comb MJ. 2007. Global survey of phosphotyrosine signaling identifies oncogenic kinases in lung cancer. *Cell* 131:1190–1203. <http://dx.doi.org/10.1016/j.cell.2007.11.025>.
35. Guo A, Villen J, Kornhauser J, Lee KA, Stokes MP, Rikova K, Possemato A, Nardone J, Innocenti G, Wetzel R, Wang Y, MacNeill J, Mitchell J, Gygi SP, Rush J, Polakiewicz RD, Comb MJ. 2008. Signaling networks assembled by oncogenic EGFR and c-Met. *Proc. Natl. Acad. Sci. U. S. A.* 105:692–697. <http://dx.doi.org/10.1073/pnas.0707270105>.
36. Rush J, Moritz A, Lee KA, Guo A, Goss VL, Spek EJ, Zhang H, Zha XM, Polakiewicz RD, Comb MJ. 2005. Immunoaffinity profiling of tyrosine phosphorylation in cancer cells. *Nat. Biotechnol.* 23:94–101. <http://dx.doi.org/10.1038/nbt1046>.
37. Stokes MP, Farnsworth CL, Moritz A, Silva JC, Jia X, Lee KA, Guo A, Polakiewicz RD, Comb MJ. 2012. PTMScan direct: identification and quantification of peptides from critical signaling proteins by immunoaffinity enrichment coupled with LC-MS/MS. *Mol. Cell. Proteomics* 11:187–201. <http://dx.doi.org/10.1074/mcp.M111.015883>.
38. Beausoleil SA, Villen J, Gerber SA, Rush J, Gygi SP. 2006. A probability-based approach for high-throughput protein phosphorylation analysis and site localization. *Nat. Biotechnol.* 24:1285–1292. <http://dx.doi.org/10.1038/nbt1240>.
39. Elias JE, Gygi SP. 2007. Target-decoy search strategy for increased confidence in large-scale protein identifications by mass spectrometry. *Nat. Methods* 4:207–214. <http://dx.doi.org/10.1038/nmeth1019>.
40. Huttlin EL, Jedrychowski MP, Elias JE, Goswami T, Rad R, Beausoleil SA, Villen J, Haas W, Sowa ME, Gygi SP. 2010. A tissue-specific atlas of

- mouse protein phosphorylation and expression. *Cell* 143:1174–1189. <http://dx.doi.org/10.1016/j.cell.2010.12.001>.
41. Yates JR, III, Eng JK, McCormack AL, Schieltz D. 1995. Method to correlate tandem mass spectra of modified peptides to amino acid sequences in the protein database. *Anal. Chem.* 67:1426–1436. <http://dx.doi.org/10.1021/ac00104a020>.
 42. Jopling C, den Hertog J. 2005. Fyn/Yes and non-canonical Wnt signalling converge on RhoA in vertebrate gastrulation cell movements. *EMBO Rep.* 6:426–431. <http://dx.doi.org/10.1038/sj.embor.7400386>.
 43. Robu ME, Larson JD, Nasevicius A, Beiraghi S, Brenner C, Farber SA, Ekker SC. 2007. p53 activation by knockdown technologies. *PLoS Genet.* 3:e78. <http://dx.doi.org/10.1371/journal.pgen.0030078>.
 44. Stewart RA, Sanda T, Widlund HR, Zhu S, Swanson KD, Hurley AD, Bentires-Alj M, Fisher DE, Kontaridis MI, Look AT, Neel BG. 2010. Phosphatase-dependent and -independent functions of Shp2 in neural crest cells underlie LEOPARD syndrome pathogenesis. *Dev. Cell* 18:750–762. <http://dx.doi.org/10.1016/j.devcel.2010.03.009>.
 45. Zhao R, Guerrah A, Tang H, Zhao ZJ. 2002. Cell surface glycoprotein PZR is a major mediator of concanavalin A-induced cell signaling. *J. Biol. Chem.* 277:7882–7888. <http://dx.doi.org/10.1074/jbc.M111914200>.
 46. Marin TM, Keith K, Davies B, Conner DA, Guha P, Kalaitzidis D, Wu X, Lauriol J, Wang B, Bauer M, Bronson R, Franchini KG, Neel BG, Kontaridis MI. 2011. Rapamycin reverses hypertrophic cardiomyopathy in a mouse model of LEOPARD syndrome-associated PTPN11 mutation. *J. Clin. Invest.* 121:1026–1043. <http://dx.doi.org/10.1172/JCI44972>.
 47. Kusano K, Thomas TN, Fujiwara K. 2008. Phosphorylation and localization of protein-zero related (PZR) in cultured endothelial cells. *Endothelium* 15:127–136. <http://dx.doi.org/10.1080/10623320802125250>.
 48. Wickstrom SA, Radovanac K, Fassler R. 2011. Genetic analyses of integrin signaling. *Cold Spring Harb. Perspect. Biol.* 3:a005116. <http://dx.doi.org/10.1101/cshperspect.a005116>.
 49. Zannettino AC, Roubelakis M, Welldon KJ, Jackson DE, Simmons PJ, Bendall LJ, Henniker A, Harrison KL, Niutta S, Bradstock KF, Watt SM. 2003. Novel mesenchymal and haematopoietic cell isoforms of the SHP-2 docking receptor, PZR: identification, molecular cloning and effects on cell migration. *Biochem. J.* 370:537–549. <http://dx.doi.org/10.1042/BJ20020935>.
 50. Bocchinfuso G, Stella L, Martinelli S, Flex E, Carta C, Pantaleoni F, Pispisa B, Venanzi M, Tartaglia M, Palleschi A. 2007. Structural and functional effects of disease-causing amino acid substitutions affecting residues Ala72 and Glu76 of the protein tyrosine phosphatase SHP-2. *Proteins* 66:963–974. <http://dx.doi.org/10.1002/prot.21050>.
 51. Walter AO, Peng ZY, Cartwright CA. 1999. The Shp-2 tyrosine phosphatase activates the Src tyrosine kinase by a non-enzymatic mechanism. *Oncogene* 18:1911–1920. <http://dx.doi.org/10.1038/sj.onc.1202513>.
 52. Peng Z-Y, Cartwright CA. 1995. Regulation of the Src tyrosine kinase and Syp tyrosine phosphatase by their cellular association. *Oncogene* 11:1955–1962.
 53. Zhang SQ, Yang W, Kontaridis MI, Bivona TG, Wen G, Araki T, Luo J, Thompson JA, Schraven BL, Philips MR, Neel BG. 2004. Shp2 regulates SRC family kinase activity and ras/erk activation by controlling csk recruitment. *Mol. Cell* 13:341–355. [http://dx.doi.org/10.1016/S1097-2765\(04\)00050-4](http://dx.doi.org/10.1016/S1097-2765(04)00050-4).